Neuromodulatory influences on propagation of brain waves along the unimodal-transmodal gradient

Verónica Mäki-Marttunen [1], Sander Nieuwenhuis[1]

[1] Cognitive Psychology Unit, Faculty of Social Sciences, Leiden University, Wassenaarseweg 52 2333 AK, Leiden, Netherlands.

Abstract

Brain activity fluctuates over time, and understanding the factors that influence such fluctuations is important to understand the flexible nature of the brain and cognition. Growing evidence suggests that fMRI brain activity shows spatio-temporal patterns of propagation following specific gradients. In particular, activity around global peaks propagates as a travelling wave following a gradient from unimodal to associative areas. Some properties of these travelling waves seem to be related to behavioral and arousal states, however their meaning remains unknown. Here we assess the possibility that travelling waves explain the finding that there are specific time points when the brain presents larger brain integration. We reasoned that a faster speed of propagation would be related to more brain integration as measured with fMRI. Furthermore, we explored whether increased pupil-linked arousal, which has been related to more integration in specific brain regions, would be increased during periods of whole brain propagation. To test these hypotheses, we detected brain travelling waves and characterized them in terms of speed, directionality and ratio. We compared these features between different task conditions, and after a pharmacological challenge affecting neuromodulatory tone. We then studied the relation between travelling wave speed, pupil size and a graph-based measure of brain integration. Our results suggest that neuromodulatory tone affects travelling wave propagation, and that this propagation reflects changes in arousal and integrated functional connectivity features. This study provides a novel view of brain dynamics in terms of the effects of neruomodulatory influences across time scales.

Introduction

A still burning question in neuroscience is how the brain maintains high flexibility and adaptability to deal with external and internal demands despite a relatively fixed anatomical structure (Yin and Kaiser, 2021). To answer this question, the field of brain dynamics has grown significatively in the past decade (Lurie et al. 2020, Iraji et al. 2021, Keilholz et al. 2017, Hutchison et al. 2013, Calhoun et al. 2014, Cabral et al. 2014, Engel and Steinmetz 2019). Studies using functional magnetic resonance imaging (fMRI) initially focused on measures of functional connectivity, showing how correlations in blood oxygen level-dependent (BOLD) activity across multiple brain regions change over time (Allen et al. 2014, Chang and Glover 2010, see Preti et al. 2017 for a review). One key aspect that emerged from that work was that, over the course of an experiment, brain activity fluctuates between periods of network-level integration and periods of network-level segregation, that is, periods when the correlation of the signal across modules is stronger

or weaker (Betzel et al. 2016, Keilholz et al. 2013, Shine and Poldrack 2018). These dynamics have been associated with the flexible nature of mental experience (MacDowell et al. 2022), but how states of integration and segregation correspond to neural events in global brain activity is still unclear.

In the past years, research on whole-brain dynamics in animals and humans has begun to directly examine fluctuations in the BOLD signal (in rodents: Liu and Zhang 2019, Mitra et al. 2018, Vafaii et al. 2024, MacDowell and Buschman 2020; in humans: see Meyer-Baese et al. 2022 for a review). Growing evidence using a variety of approaches suggests the presence of propagating waves at a macroscopic scale and in the slow frequencies (Matsui et al. 2016, Raut et al. 2020, Yousefi and Keilholz 2021), which appear to be relevant for cognition (Xu et al. 2023). In particular, a number of fMRI and electrophysiology studies in rodents, primates and humans suggests that activity seems to propagate through the brain as travelling waves following a gradient from unimodal to associative areas (Matsui et al. 2016, Gu et al. 2021). An interesting possibility has thus been suggested that the propagation of activity across this gradient could give rise to some of the hallmark findings in studies of functional connectivity (Shahsavarani et al. 2023, Raut et al. 2023). The canonical approach of identifying correlated "networks" of activity may be influenced by the position of these networks along what is actually a continuous gradient underlying observed travelling waves. If this is the case, one prediction would be that a change in the *speed of propagation* must cause variations in the correlation between networks, which would be reflected in changes in overall integration (Mäki-Marttunen 2023). That is, if activity propagates faster, it would result in more temporal alignment between regions' time courses, manifested as higher integration. Finding such evidence would lend further support for the slow propagation of activity as a comprehensive framework to study brain dynamics and for our understanding of the factors that make the brain highly flexible.

What can cause changes in the propagation speed of travelling waves? One possible factor is the level of neural excitability as set by neuromodulatory systems (Raut et al. 2023). Neuromodulatory systems such as the dopamine system and noradrenaline system work at fast and slow time scales and influence large parts of the brains with their wide-spread projections (McCormick et al. 2020, van den Brink et al. 2019). It is well known that low levels of neuromodulatory tone are related to lower excitability and more neural synchronization, while intermediate levels are related to higher excitability and responsivity, and an overall desynchronization (Aston-Jones and Cohen 2005). A computational study has assessed the effect of excitability on travelling waves, and they found that larger excitability was associated with faster propagation (Bhattacharya et al. 2021). Studies in humans offer indirect evidence, by showing that increases or decreases in pupil size during the course of an experiment are associated with more or less brain integration, respectively (Shine 2019, Shine et al. 2016, Mäki-Marttunen 2021). However, a relation between neuromodulation, global brain activity dynamics and measures of integration remain untested in the context of macroscopic travelling waves in the human brain.

In the current study, we aimed to test these hypotheses in a concurrent fMRI-pupillometry study including a pharmacological challenge of neuromodulatory systems. We first detected travelling waves and characterized them in terms of speed, directionality and ratio of top-down and bottom-up propagations. We compared these features between resting state and task performance, and after placebo or atomoxetine manipulation. Atomoxetine is a blocker of the noradrenaline transporter and is associated with an increase in the free levels of catecholamines (i.e. dopamine and noradrenaline, (Bymaster et al., 2002; Swanson et al., 2006; Koda et al., 2010). We then studied the relation between travelling waves, pupil size (a measure of neuromodulatory arousal; Joshi and Gold, 2020, Lloyd et al., 2023) and the participation coefficient, a graph-based measure of brain integration that is sensitive to fluctuations in

neuromodulatory inputs (Shine et al. 2016, 2018, Mäki-Marttunen 2021). Based on the predictions laid out by Mäki-Marttunen (2023), we hypothesized that (i) pharmacollogically increased levels of catecholamines would be associated with faster travelling waves, that (ii) faster travelling wave speed would be associated with a more integrated network state, and that (iii) the presence of travelling waves would be associated with larger pupil size. Our results provide the first evidence in humans that neuromodulation is related to global brain activity propagation and that these events have explanatory power regarding the findings on varying levels of integration across functional networks. This study is an important step towards understanding how neuromodulatory systems endow the brain with a large flexibility by modulating patterns of global communication.

Methods

Participants

36 individuals (average age: 23 years old, range: 18–29 years, 14 male) were recruited and medically screened by a physician for physical health and drug contraindications. Exclusion criteria included: standard contraindications for MRI; heart arrhythmia; glaucoma; hypertension; use of antidepressants or psychotropic medication; history of psychiatric illness or head trauma; drug or alcohol abuse; learning disabilities; poor eyesight; smoking more than 5 cigarettes a day; consumption of more than 24 units of alcohol; and pregnancy. All participants gave written informed consent before the experiment and were compensated with €110.

Study design and MRI data acquisition.

The study had a double-blind placebo-controlled crossover design. In each of two sessions, scheduled 1 week apart at the same time of day, participants received either a single oral dose of atomoxetine (40 mg) or placebo (microcrystalline cellulose PH 102, visually identical to the drug). Participants had a waiting time after pill ingestion, to allow for atomoxetine concentration to reach peak plasma levels. During the waiting interval, they either practiced the tasks (first session) or engaged in some quiet activity of their choice. The tasks employed in this study took place from about 90 minutes after pill ingestion.

All MRI data were collected with a Philips 3T MRI scanner. In the beginning of each of the scanning sessions, we collected a high-resolution anatomical T1 image (echo time 3.5 ms, repetition time 7.99 ms, flip angle 8°, and FOV 250 195 170 mm with voxel size of 1.1 mm isotropic). Functional scans consisted on T2*-weighted EPI images (echo time 30 ms, repetition time 2.2 s, flip angle 80°, FOV 220 220 120 mm of size 2.75 mm isotropic). Eye tracking data were collected during the fMRI scans using an MRI-compatible EyeLink device. The camera was set to image the right eye and a calibration was carried out soon after the participant entered the scanner. The eye-tracking recordings were sampled at a frequency of 1000 Hz. Each scanning session lasted about 90 minutes.

Tasks and stimuli

In the scanner, participants underwent two resting state fMRI runs, and performed one run of a continuous performance task, and one run of a movie watching task. During the resting state scan, participants were instructed to fixate their eyes on a black cross on a gray background. In the a continuous performance task they were presented with a stream of images of cities and mountains, and had to mentally count the number of pictures with mountains. The stimuli consisted of 10 pictures of cities and

10 pictures of mountain landscapes that were presented multiple times in random order across the run. A key characteristic was that the transition between images was softened by making images fade into the next, which ensured a "continuous" type of stimulation. The images subtended approximately 6 degrees of visual angle, were isoluminant, grayscale, and were presented on a gray background. The images linearly and continuously morphed from one into the next, with an 800-ms interval (van den Brinket al. 2016). The percentage of mountains in the first session was set to 10% and on the second session to 40%. After the run, participants were asked how many mountains they had counted. The participants also performed a naturalistic viewing task which involved watching a shortened version of Hitchcock's episode "Bang". This clip has been widely used in fMRI experiments because it includes moments of suspense associated with specific brain patterns that can be observed across subjects (Naci et al. 2014). The clip included sound and subtitles. All functional runs (resting and tasks) lasted approximately 8 minutes. The tasks were coded with Psychtoolbox running on MATLAB.

Pupillometry preprocessing and analysis

Raw eye-tracking data were converted to asc files using the EDF2ASC converter. Preprocessing of the pupil signal consisted on interpolation of pupil blinks, normalization, detrending, and downsampling to the scanner frequency. Coding of these steps was based on code provided by Urai et al. (2017). Cross-correlation between pupil size and global signal was calculated with the function *xcorr* (MATLAB) as c = xcorr(global signal, pupil). We also analyzed identified *pseudo-events* in the resting-state pupil data, using the point process approach implemented in the RS-HRF toolbox (Wu et al. 2021). Briefly, the tool identifies the points where the signal exceeds 1 standard deviation, and fits an impulse response function. Thus, the *pupil events* are defined as pupil change that resemble an evoked response identified around points of high pupil signal. The RS-HRF toolbox allowed us to get the time points at which pupil events were detected. We calculated the proportion of pupil pseudo-events per time length of the intervals around global signal peaks (see below), because slower waves are expected to be related to longer intervals that may include more pupil events.

fMRI preprocessing and analysis

Data were preprocessed using a standard pipeline implemented in FMRIPrep version xx (Esteban et al. 2018, fmriprep.org), including slice-time correction, image realignment, deconfounding of movement regressors and mean signal of white matter and cerebrospinal fluid, detrending, and normalization to MNI space. Further steps included filtering (0.001-0.1 Hz) and z-scoring of the voxels' timecourses. The analysis of brain activity propagation was done in surface space.

To study brain activity propagation along the principal gradient, we followed the procedure by Gu et al. (2021) and adapted the code shared by the authors. Briefly, the approach consists of, first, identifying the peaks of the global signal and the intervals around each of these peaks (i.e. from the trough before to the trough after each peak), and second, obtaining the time difference between peaks in the timecourses of the voxels with respect to the peak in the global signal, that is, the *delay values* (Figure I). The vectors of delay values for all participants and scans were entered into a singular value decomposition algorithm. We then examined the first five main components (Figure I) and identified the one corresponding to the *principal gradient*, that is, the one where brain regions are organized following a unimodal-transmodal gradient. Figure I shows the correlation between the vectors of delay values for all intervals considered and the vector corresponding to the principal gradient component. A bimodal distribution with a higher number of values in negative and positive correlations as compared to no correlation (zero value)

indicates the presence of travelling waves in bottom-up and top-down directions along the gradient, respectively.

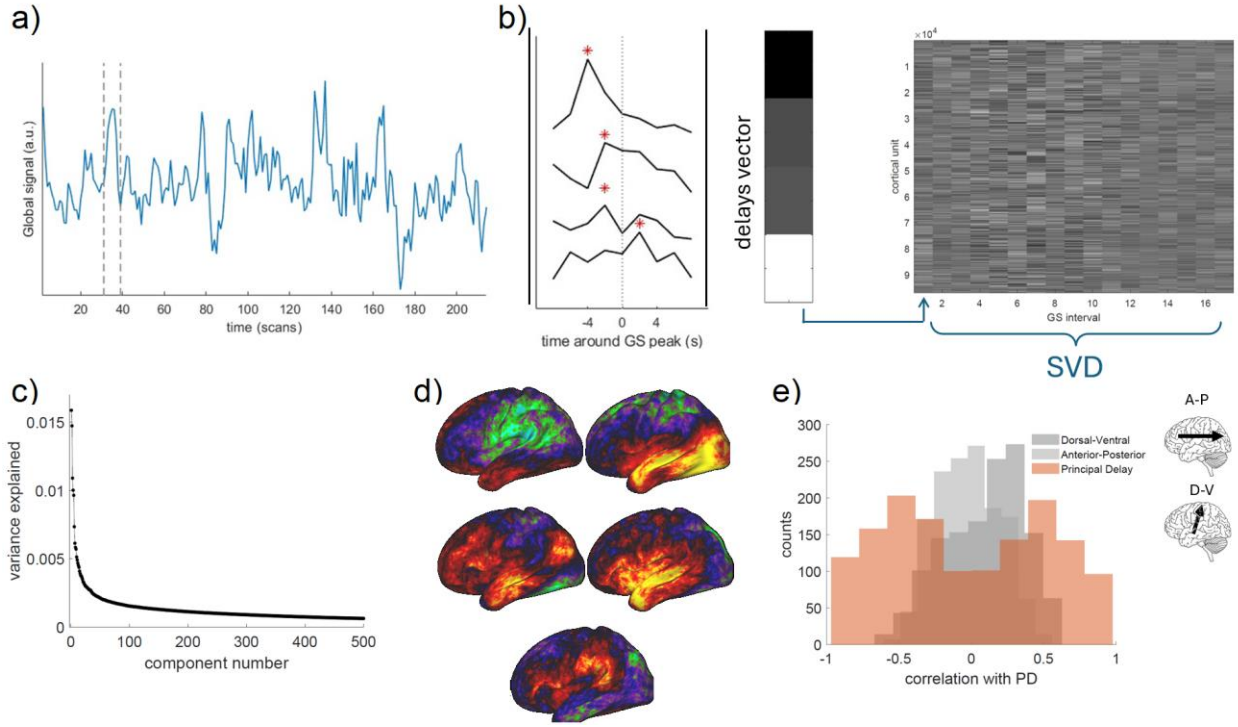

Figure I. Calculation of main delay component. a) Example of extraction of delay vector from one session. The peaks of the global signal were identified (left) and b) the time difference between the peak of activity of each voxel and the global peak were calculated, resulting in one vector of delay values per interval (middle). The delay vectors were concatenated for all participants, sessions and tasks (right), and the matrix was submitted to a singular value decomposition analysis). c) Variance explained by each component. d) Brain maps corresponding to the first five components. The left map on the middle row (component #3) corresponds to the principal gradient. e) Histogram of correlation values between the delay vectors and the main delay component (red). The histograms corresponding to the anterior-posterior (A-P) and dorsal-ventral (D-V) gradients are also plotted. Brain insets indicate A-P and V-D directionality.

To study activity propagation along this gradient, for each individual and run, the voxels were ordered according to the gradient (i.e. from unimodal to multimodal) and binned in 30 bins to reduce the dimensionality of the analysis. The BOLD signal for each bin (i.e. averages over voxels) was used to study travelling waves (see a participant's data example in Figure I). Following Gu et al. (2021), we based the analyses on intervals of global involvement, for example those intervals where the global signal (averaged over all gray matter voxels) was larger than the peaks identified from a null distribution (i.e. based on shuffled data). To compute the speed of the waves, we used the formula as in Gu et al. (2021):

$$\text{Speed} = |c| * \text{geodesic distance (mm)} / \text{n bins} / \text{TR (s)}$$

where the coefficient *c* corresponds to the linear fit where the position of the peak in the BOLD signal for each bin is regressed against bin number. A positive coefficient corresponded to a propagation from unimodal to transmodal areas (bottom-up), and a negative coefficient corresponded to a propagation from transmodal to unimodal (top-down). Figure II shows the average travelling waves in each direction. We set a threshold for the identification of travelling waves based on the distribution of coefficients for

the two other propagation directions (A-P and V-D). The threshold was set at alpha = 0.1 and corresponded to a coefficient of absolute value 3.8 (Figure II.d).

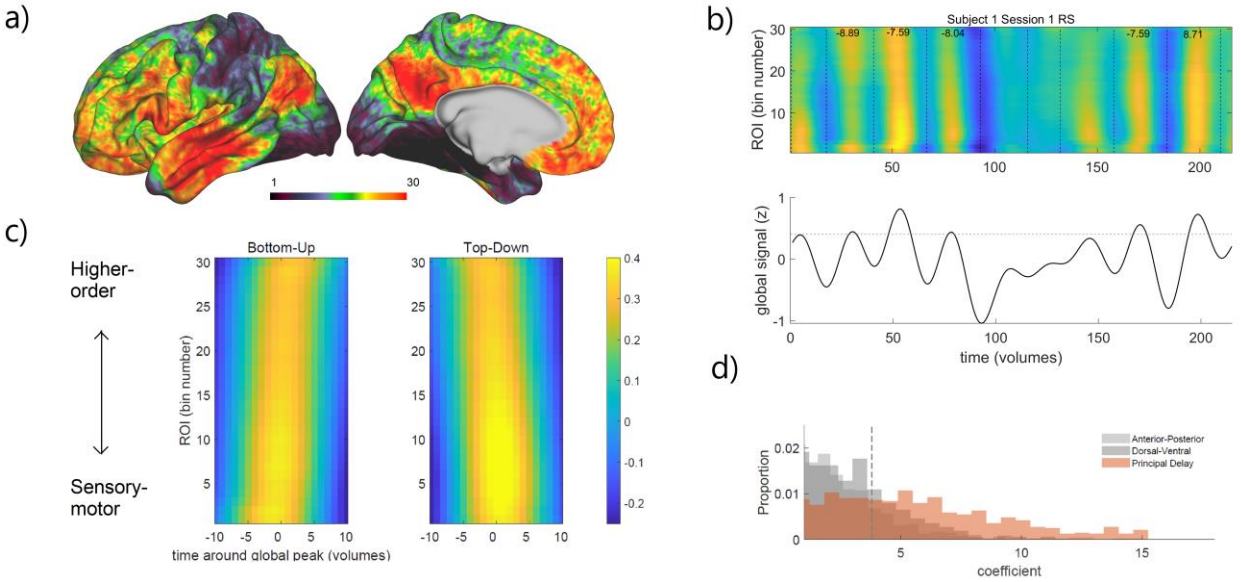

Figure II. Calculation of speed of travelling waves. a) Map of principal delay component, binned into 30 parcels according to delay with respect to the global signal peak. b) Example of one participant's scan where signal of the regions of interest after the principal delay is plotted (top panel). The travelling waves can be observed in relation to the global signal peaks (bottom panel). Horizontal line indicates significance threshold for global signal peaks obtained from permutation testing. c) Average bottom-up and top-down travelling waves across participants and conditions. d) Distribution of travelling wave coefficients for the two control directions and the principal delay direction. Threshold obtained from permutation testing is indicated with a vertical dashed line.

For the calculation of brain topological variables, we used the Gordon 333 parcellation (Gordon et al. 2016, Figure VI.a). In the Gordon 333 parcellation, each parcel is assigned to one of twelve different networks: Default, Parieto-Occipital, Fronto-Parietal, Salience, Cingulo-Opercular, Medial-Parietal, Dorsal-Attention, Ventral-Attention, Visual, Somatomotor hand, Somatomotor mouth, and Auditory. To account for the fact that the waves were related to peaks in global signal, which could inflate the estimation of integration measures, the global signal was regressed out from each voxel's timecourse. Data for all voxels within a parcel were averaged. The temporal segments corresponding to the intervals with travelling waves were used to calculate the correlation coefficient between each pair of parcels, resulting in a connectivity matrix. The network assignments were used as modules for the calculation of within-module and between-module connectivity on the connectivity matrices, as well as the participation coefficient, a measure of brain integration. The participation coefficient was calculated as the average of the weights of a given parcel to each module with respect to all the weights of the parcel. For calculating the participation coefficient, we used the Brain Connectivity Toolbox (Rubinov and Sporns, 2010, https://sites.google.com/site/bctnet).

Statistics

We were interested in the effect of treatment (atomoxetine vs. placebo) and behavioral state (rest vs. task-engaged) on travelling waves, and so we combined the data for the two resting state scans and compared them with the aggregated data from the two tasks. We ran repeated-measures ANOVAs with

propagation speed or top-down to bottom-up ratio as the dependent variable, and treatment and behavioral state as within-subject factors. For the analysis of propagation speed, we also included wave direction (top-down vs. bottom-up) as a within-subject factor. For the analysis of pupil-linked arousal, we ran a repeated-measures ANOVA with mean pupil size in a given time interval as the dependent variable, and treatment, behavioral state, and presence/direction of travelling waves (none, bottom-up, top-down) as within-subject factors. To test for a relation between propagation speed, mean pupil size, number of pseudo-pupil events (underlying the resting-state pupil signal), and measures of network-level integration, we ran a linear regression for the tested pair of variables, and included treatment and behavioral states as additional predictors. In these analyses we included all intervals, not only those of significant global involvement, so teh correlations covered the whole range of variation in the pupil and integration variables. The linear models were coded using lme function in MATLAB.

Results

Effects of atomoxetine and behavioral state on brain activity propagation

First, we defined intervals around peaks in the global signal. Within those intervals, we then calculated the delay values of each voxel with respect to the global signal peak (delay profile). We finally applied singular value decomposition to those delay profiles to identify the main gradient of delays (Figure I; Figure III.c displays distribution of correlation values between the delay profiles and the principal gradient). For this, we used the whole dataset, including both treatments and behavioral states. Then, we binned the voxels into 30 equally-sized bins along the principal gradient and identified the bottom-up and top-down waves of activity propagation over the main delay profile in those intervals.

To test our hypothesis that pharmacologically increased levels of catecholamines would be associated with faster travelling waves, we compared the propagation speed of bottom-up and top-down waves in the various conditions by performing a RM-ANOVA with the within-subject factors treatment, behavioral state and wave direction (bottom-up, BU, and top-down, TD). This analysis yielded a significant treatment effect ($F(252) = 5.61$, $p = 0.018$, Table I). Speed was faster under atomoxetine as compared to placebo (Figure III.a,b, Table I), confirming our hypothesis. We found no effect of behavioral state or wave direction. Next, we compared the ratio of top-down to bottom-up travelling waves between conditions. This ratio significantly differed between behavioral states ($F(110) = 10.50$, $p = 0.001$), with smaller TD:BU ratio, that is, relatively more bottom-up waves, during task performance than RS (Figure III.d). The ratio was numerically lower under atomoxetine as compared to placebo, but this effect was not significant (Table I).

	Speed		**TD:BU ratio**	
Effect	**F**	**P value**	**F**	**P value**
Task	1.28	0.257	10.54	**0.001**
Treatment	5.61	**0.018**	3.39	0.068
Direction	1.96	0.16		
Task*Treatment	0.19	0.661	0.01	0.907
Task*Direction	0.18	0.670		
Treatment*Direction	0.04	0.828		

Table I

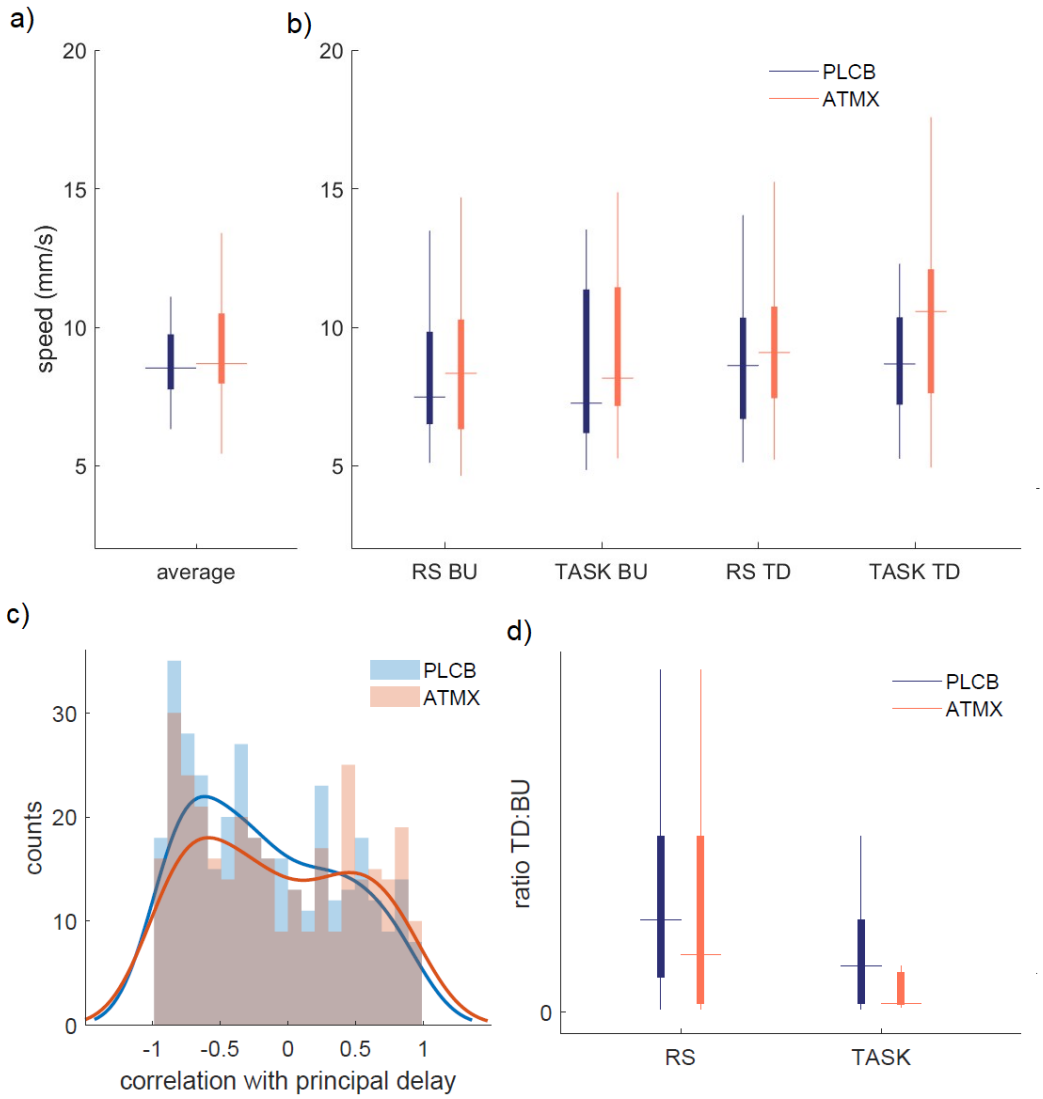

Figure III. Travelling waves speed and ratio across conditions and treatment. a) Speed of travelling waves in the two different treatment conditions and b) separated by treatment, behavioral state and wave direction. c) Histogram of correlation values between the delay vectors of the individual windows with travelling waves and the principal delay vector. d) Ratio of top-down (TD) to bottom-up (BU) waves per condition and treatment. In the boxplots, the central mark is the median, the edges of the box are the 25th and 75th percentiles, the whiskers extend to the most extreme datapoints. PLCB: placebo. ATMX: atomoxetine. RS: resting state.

Relationship between brain activity propagation and pupil-linked arousal

To study the relation between pupil size and brain dynamics, we investigated the slow fluctuations in pupil signal filtered with the same band-pass filter as the BOLD global signal (0.001-0.01 Hz). These fluctuations reflect slow changes in activity of these neuromodulatory nuclei (Joshi & Gold, 2020; Lloyd et al., 2023, Figure IV.a). We found that the global signal and the filtered pupil signal were cross-correlated with a lag of around –5 scans (11 seconds), with fluctuations in the global signal preceding the corresponding

fluctuations in pupil size (Figure IV.d). This direction is consistent with previous reports in mice (Pais-Roldán et al. 2020). The presence of several significant intervals may show certain periodicity in the signals. The cross-correlation was largely consistent across behavioral states and treatments. We also investigated pupil-related *pseudo-events*, latent neural events that were estimated to underlie large (i.e., seemingly evoked) changes in the resting-state pupil signal (Figure IV.b, see Methods). We assumed that these were time points associated with phasic bursts of activity in nuclei of the ascending arousal system, including the locus coeruleus (Munn et al., 2021). The pseudo-events were only obtained in the resting state scans to avoid stimuli-related pupil effects. We found that the pseudo-events clustered around global signal peaks, and in particular after the peak (Figure IV.c).

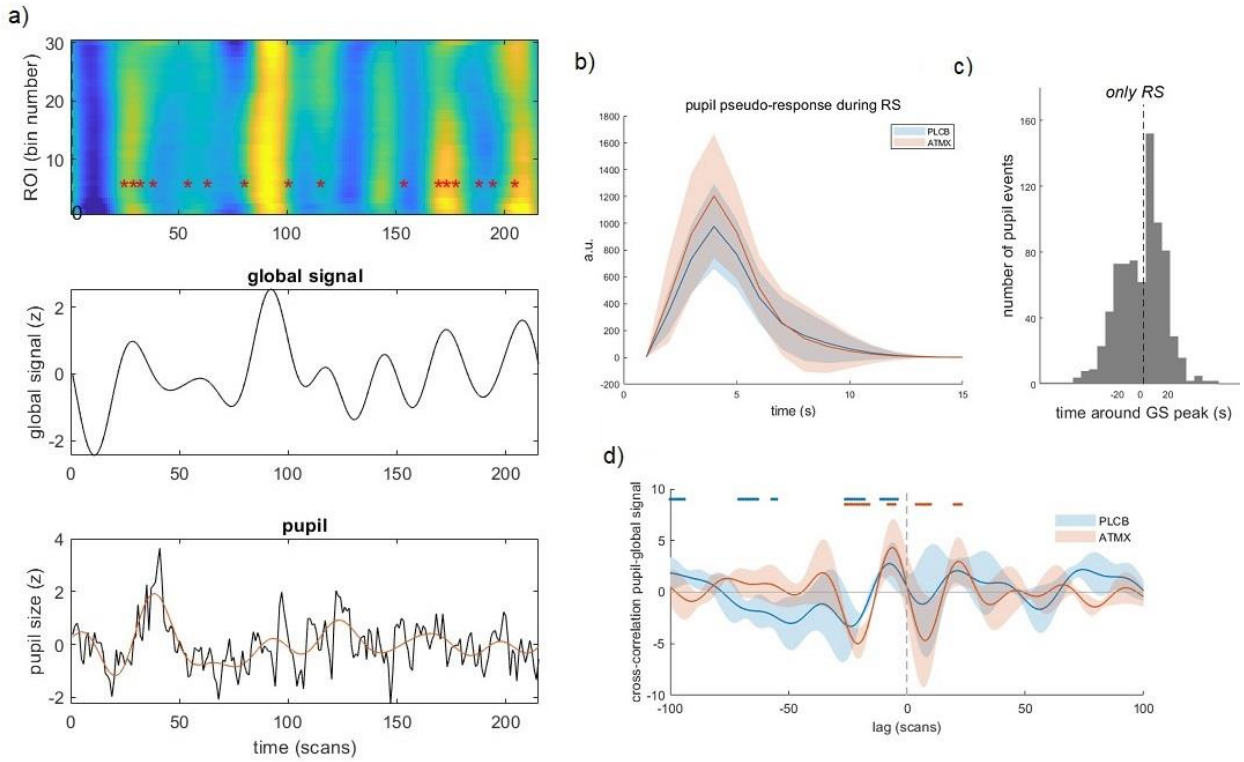

Figure IV. Relation between pupil size and global signal. a) A sample participant's run. Top panel: brain activity ordered by the principal gradient with identified pupil-related pseudo-events (estimated from the resting-state pupil data) overlaid as red asterisks. Middle panel: global signal. Bottom panel: Pupil signal resampled to the fMRI sampling rate (black) and the low-passed pupil signal (red). b) Average of the phasic events that were deconvolved to estimate the underlying neural pseudo-events. c) Histogram of distribution of fast pupil events around global signal peaks. d) Average raw cross-correlation between pupil and global signal for the different treatment effects. PLCB: placebo. ATMX: atomoxetine. RS: resting state. GS: global signal.

To test our hypothesis that the presence of travelling waves would be associated with larger pupil size, we compared between intervals with (bottom-up or top-down) and without travelling waves. We found a significant effect, with larger pupil size in intervals with bottom-up or top-down travelling waves (Figure V.a, presence of waves effect: $F(277) = 4.19$, $p = 0.041$), confirming our hypothesis. Note that the

variability of mean pupil size was also larger for intervals with travelling waves. We then tested the relation between our pupil-related variables (mean pupil size and proportion of pupil pseudo-events, Figure V) and propagation speed. Propagation speed was not associated with mean pupil signal ($F(1034) = 0.05$, $p = 0.822$) but was significantly associated with proportion of pseudo-events ($F(471) = 4.40$, $p = 0.036$), whereby intervals with larger speed were associated with less pseudo-events. No effect of treatment was observed in these analyses (mean pupil, treatment effect: $F = 0.12$, $p = 0.723$, behavioral state effect: $F = 0.02$, $p = 0.877$; pseudo-events, $F = 0.049$, $p = 0.484$). Taken together, the results suggest that time periods with traveling waves were characterized by larger mean pupil-linked arousal, and that speed of travelling waves was negatively associated with pupil pseudo-events.

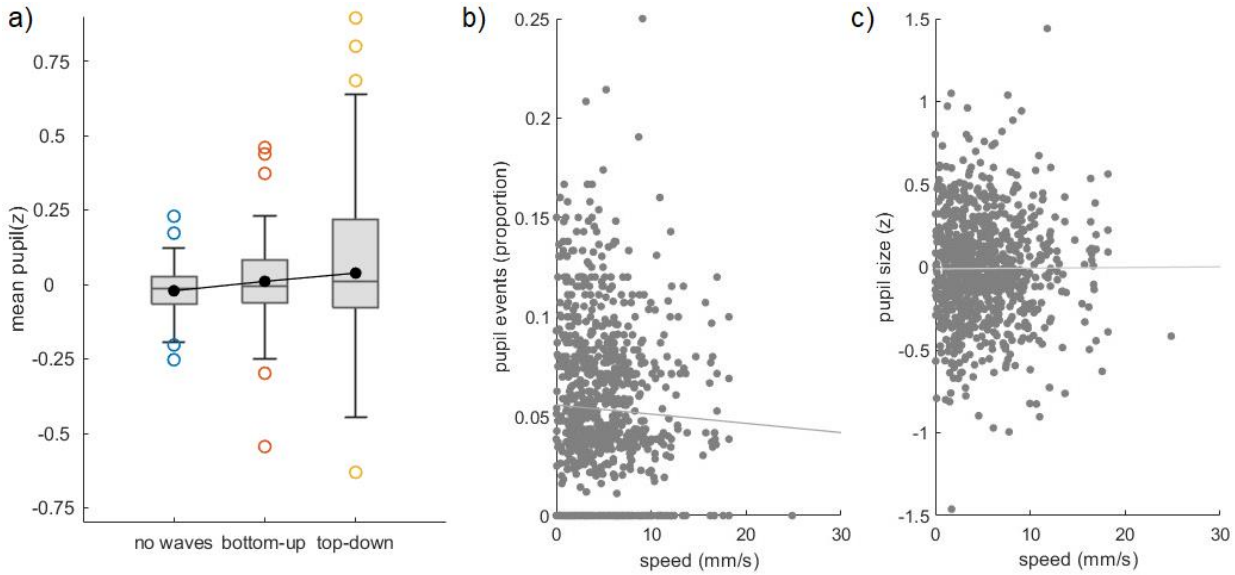

Figure V. Links between travelling waves and pupil-linked arousal. a) Relation between presence/direction of travelling waves and mean pupil size. b) Relations between propagation speed and pupil measures. Each observation represents one interval.

Relation between brain activity propagation and network topology

To test the hypothesis that that faster travelling wave speed would be associated with a more integrated network state, we calculated participation coefficient, a measure of integration. For this, we used the Gordon parcellation that divides up the cortex into 333 parcels (Figure VI.a) and averaged the data from all voxels within each parcel. Each parcel is assigned to a resting state network, and this assignment was used to compute the participation coefficient. We found that propagation speed was positively related to the level of integration (Figure VI.b; $F(683) = 97.79$, $p < 0.001$), confirming our hypothesis. There were no significant effects of treatment ($F = 0.01$, $p = 0.925$) and behavioral state ($F = 0.74$, $p = 0.387$) on level of integration. We also tested for a relation between pupil size and integration. We categorized all time intervals into four bins on the basis of mean pupil size and tested for an effect on the participation coefficient, following the procedure used in Mäki-Marttunen (2021). We found that larger pupil size was related to higher network integration, with the exception of the largest pupil bin, resulting in an inverted U shape (Figure VI.b, pupil bin linear effect: $F(396) = 14.35$, $p < 0.001$, pupil bin quadratic effect: $F(396) =$

13.83, $p < 0.001$). In sum, network integration was positively related to propagation speed and pupil size, the latter presenting also non-linear effects.

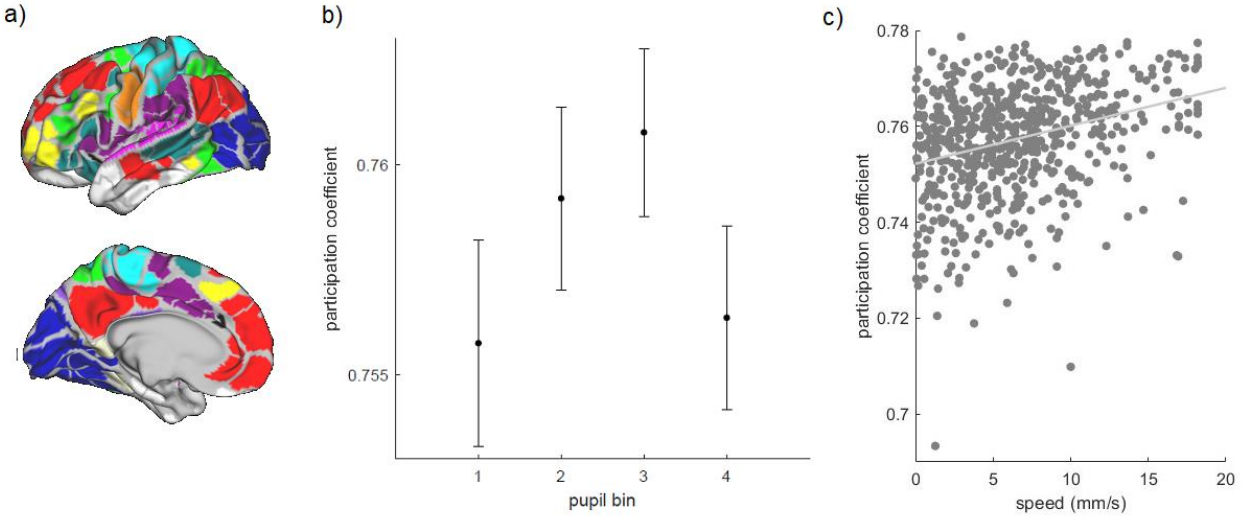

Figure VI. Brain integration. a) 333 parcells (Gordon et al. 2016) were used to calculate the participation coefficient, a measure of brain integration. b) Relation between pupil size and network integration. c) Relation between propagation speed and network integration.

Discussion

The current study aimed to investigate whether neuromodulation has some enabling role on global activity propagation. We thus examined whether macroscopic patterns of brain activity could account for the findings that the organization of brain "networks" appears to fluctuate into more/less integrated states, and that these are related to increased/decreased pupil size, respectively. For this, we studied whether the travelling waves were related to measures of brain integration, and whether they were affected by neuromodulatory levels. We had hypothesized that increased levels of catecholamines would be associated with faster travelling waves, that faster waves would be associated with a more functionally integrated brain, and that larger pupil size would be associated with the presence of travelling waves. We found that travelling waves were faster under atomoxetine, and that faster travelling waves were related to more integration in functional connectivity. We also found that travelling waves were related to intervals of larger pupils on average. In sum, we found evidence in favor of the hypothesis that whole brain activity patterns underlie the findings relating to functional connectivity and integration, and its neuromodulation by pupil-linked arousal systems. This has important implications for the understanding of the brain mechanisms that underlie the dynamic properties of the human brain.

Travelling waves

Here we examined the presence of travelling waves by extracting a main delay component of BOLD signal based on intervals determined by global signal peaks and troughs, as in Gu et al. (2021). This method allowed us to obtain the main component that reproduces the main gradient of the brain, which separates unimodal from associative areas, and has been found across modalities and using different approaches (see Huntenburg et al. 2018 for a review). Propagation of activity in the form of travelling waves has been

observed also in rodents and monkeys (Mitra et al. 2018, Matsui et al. 2016, Gu et al. 2021, Raut et al. 2021), indicating that they constitute a ubiquitous phenomenon. As previously reported, we found propagation of activity both bottom-up and top-down. Importantly, we could detect them across the three behavioral states employed here, resting state, continuous performance task, and movie watching. This is consistent with a previous study that found underlying patterns of activity following the principal gradient in resting state and a variety of tasks (Brown et al. 2022). An important difference is that in our study, none of the tasks required an active motor response or were paced as in event designs, and thus could be considered as "continuous" state, which made them comparable with the resting state in terms of design. We found a task effect on travelling wave ratio, where tasks were associated with a larger proportion of bottom-up travelling waves across treatment conditions. Since the tasks had a strong visual component, it is possible that this effect depended on the quality of the task (Brown et al. 2022). The atomoxetine manipulation was related to a larger proportion of bottom-up waves as compared to placebo, but this effect was non-significant ($p = 0.068$). A significantly larger proportion of bottom-up as compared to top-down travelling waves was found in sleepy individuals, as well as in monkeys (Gu et al. 2021). Recent studies using a serotoninergic agonist found that the principal gradient is contracted with increasing levels of serotonin (Girn et al. 2022, Timmermann et al., 2023). Taken together, the results suggest that neuromodulatory factors have an effect on the directionality of propagation of travelling waves along the principal gradient, reflecting the expression of a variety of brain states.

Global brain activity, brain integration and neuromodulation

A key finding was that the speed of travelling waves was significantly higher in the atomoxetine condition across tasks (Figure III). Computational studies suggest that one mechanism by which neuromodulatory systems influence the speed of travelling waves is by altering the overall excitability of the brain (Bhattacharya et al. 2021). Noradrenaline and dopamine systems, which are directly affected by noradrenaline transporter blockade with atomoxetine (Bymaster et al., 2002; Swanson et al., 2006; Koda et al., 2010), affect neuronal activity through binding to a variety of receptors distributed over the cortex (Aston-Jones and Waterhause, 2016; Avery and Krichmar, 2017; Rho et al. 2018). In particular, atomoxetine increases neuronal excitability (Bymaster et al., 2002; Koda et al., 2010; DiMiceli et al. 2015). Contrary to early views that noradrenaline affects all brain regions homogeneously, an interesting fact is that the receptors have different affinities and are distributed differentially over the cortex and the cortical layers (O'Donnell et al. 2012). In addition, projections from the noradrenergic nucleus locus coeruleus (LC) appear to present some level of modularity, where LC cells conform ensembles that project to the same region (Chandler et al. 2019). Taken together, the findings point towards levels of neuromodulatory activity exerting a nuanced modulation of brain propagation, rather than or in addition to having a spatial or temporal unspecific effect on cortical activity (Totah et al. 2018).

Studies using pupillometry concurrent with fMRI found that periods of larger pupil were related to more integration (Shine et al. 2016, Mäki-Marttunen 2021). Atomoxetine manipulation has also been related to an effect on the brain's integration/segregation balance (Guedj et al. 2016, van den Brinck et al. 2016, 2018, Shine et al. 2018). Different measures of brain integration were used across studies, which may underlie some differences in the direction of the effect. Our approach allowed us to look at neuromodulatory effects on a temporally finer perspective by looking at the travelling waves over the principal gradient. The results revealed that periods of more integration may in part follow changes in speed of activity propagation across the principal gradient, and these may relate to fluctuations in neuromodulatory tone. Fluctuations in brain integration and segregation have been described within

single scan sessions (Betzel et al. 2016, Keilholz et al. 2013, Shine and Poldrack 2018). Furthermore, several studies reported that there are specific time points that contribute the most to the phenomena of functional connectivity (Tagliazucchi et al. 2012; Liu and Duyn 2013). Our results allow tying together these lines of findings by suggesting that the 1) modulation of macroscopic brain activity by level of neuromodulators may be not only in terms of a change in the overall state of brain connectivity but also in terms of the temporal relation of activity propagation across regions following the unimodal-transmodal hierarchy, 2) the effects of neuromodulatory activity on brain propagation may in turn underlie the phenomena of fluctuating brain integration over time through modulation of propagatory events, and 3) these single events of brain propagation may be the ones contributing to the emergence of brain functional connectivity. While further studies may strengthen these hypotheses, our findings offer a finer picture of task-unrelated neuromodulatory effects on brain function.

We also found that larger pupil size was related to more integration, although integration dropped at the largest pupil size values, following an inverted-U curve. At least in a certain range of pupil size, we replicated a positive relation between pupil size and brain integration, as measured with participation coefficient (Mäki-Marttunen 2021). We did not find an effect of pupil size on speed, but found a significant negative association between speed and number of pupil events. Pupil pseudo-events co-occur with BOLD changes in neuromodulatory regions in fMRI (Lloyd et al. 2023). While we can only speculate on the meaning of this finding, it is possible that time intervals of faster travelling waves are related to less variability in neuromodulatory nuclei and thus pupil events. While more work is needed to test for a relation between travelling waves and pupil size in other conditions and states, our results point towards a timed relation between neuromodulatory activity and global patterns of brain activity.

We also examined a possible relation between global signal and pupil size. The physiological meaning of global BOLD signal is still a matter of debate (Liu et al. 2017). The distinction between neuronal or artifactual sources of global signal changes has great relevance for the consideration of global signal removal as a preprocessing step in functional connectivity studies (Power et al. 2017). Previous studies suggest that the global signal is at least in part related to arousal level (Liu et al. 2018; Wong et al. 2013). We found a relation between pupil size and pupil events and the global signal. A temporal relation between pupil size and global signal is consistent with previous reports in mice (Pais-Roldán et al. 2020). The fact that pupil size and events peaked after the global signal may reflect an event of transient arousal following a drop in arousal (Demiral et al. 2023). Our results contribute to the understanding of global brain activity by showing that pupil-linked processes are related to fluctuations of pupil signal, and thus present arousal related influences in a time-specific manner.

Conclusions

By unveiling a relation between neuromodulatory tone, brain activity propagation along the unimodal-transsmodal gradient, and pupil size, our study allows linking together several lines of research on brain dynamics, and provides a novel view of the effects of neruomodulatory systems across time scales.

References

1. Aston-Jones G, Cohen JD. An integrative theory of locus coeruleus-norepinephrine function: adaptive gain and optimal performance. Annu Rev Neurosci. 2005;28:403-50.

2. Aston-Jones, G., & Waterhouse, B. (2016). Locus coeruleus: from global projection system to adaptive regulation of behavior. *Brain research*, *1645*, 75-78.
3. Avery, M. C., & Krichmar, J. L. (2017). Neuromodulatory systems and their interactions: a review of models, theories, and experiments. *Frontiers in neural circuits*, *11*, 108.
4. R.F. Betzel, M. Fukushima, Y. He, X.-n. Zuo, O. Sporns Dynamic fluctuations coincide with periods of high and low modularity in resting-state functional brain networks NeuroImage, 127 (February) (2016), pp. 287-297
5. Bhattacharya, M.B. Cauchois, P.A. Iglesias, Z.S. Chen. The impact of a closed-loop thalamocortical model on the spatiotemporal dynamics of cortical and thalamic traveling waves. Sci. Rep., 11 (1) (2021), pp. 1-19
6. Brown, J. A., Lee, A. J., Pasquini, L., & Seeley, W. W. (2022). A dynamic gradient architecture generates brain activity states. *NeuroImage*, *261*, 119526.
7. Bymaster FP, Katner JS, Nelson DL, Hemrick-Luecke SK, Threlkeld PG, Heiligenstein JH, Morin SM, Gehlert DR, Perry KW (2002) Atomoxetine increases extracellular levels of norepinephrine and dopamine in prefrontal cortex of rat: a potential mechanism for efficacy in attention deficit/hyperactivity disorder. Neuropsychopharmacology 27:699–711.
8. Cabral J, Kringelbach ML, Deco G. Exploring the network dynamics underlying brain activity during rest. Prog Neurobiol. 2014
9. Calhoun VD, Miller R, Pearlson G, Adalı T. The chronnectome: time-varying connectivity networks as the next frontier in fMRI data discovery. Neuron. 2014 Oct 22;84(2):262-74.
10. Chandler, D. J., Jensen, P., McCall, J. G., Pickering, A. E., Schwarz, L. A., & Totah, N. K. (2019). Redefining noradrenergic neuromodulation of behavior: impacts of a modular locus coeruleus architecture. *Journal of Neuroscience*, *39*(42), 8239-8249.
11. C. Chang, G.H. Glover Time-frequency dynamics of resting-state brain connectivity measured with fMRI. Neuroimage, 50 (1) (2010), pp. 81-98
12. Şükrü Barış Demiral, Christopher Kure Liu, Helene Benveniste, Dardo Tomasi, Nora D Volkow, Activation of brain arousal networks coincident with eye blinks during resting state, *Cerebral Cortex*, Volume 33, Issue 11, 1 June 2023, Pages 6792–6802
13. Di Miceli, M., Gronier, B. Psychostimulants and atomoxetine alter the electrophysiological activity of prefrontal cortex neurons, interaction with catecholamine and glutamate NMDA receptors. Psychopharmacology 232, 2191–2205 (2015).
14. Engel TA, Steinmetz NA. New perspectives on dimensionality and variability from large-scale cortical dynamics. Curr Opin Neurobiol. 2019 Oct;58:181-190.
15. Esteban O, Markiewicz CJ, Blair RW, Moodie CA, Isik AI, Erramuzpe A, Kent JD, Goncalves M, DuPre E, Snyder M, Oya H, Ghosh SS, Wright J, Durnez J, Poldrack RA, Gorgolewski KJ. fMRIPrep: a robust preprocessing pipeline for functional MRI. Nat Meth. 2018.
16. Girn, M., Roseman, L., Bernhardt, B., Smallwood, J., Carhart-Harris, R., & Spreng, R. N. (2022). Serotonergic psychedelic drugs LSD and psilocybin reduce the hierarchical differentiation of unimodal and transmodal cortex. *NeuroImage*, *256*, 119220.

17. Gordon EM, Laumann TO, Adeyemo B, Huckins JF, Kelley WM, Petersen SE. Generation and Evaluation of a Cortical Area Parcellation from Resting-State Correlations. Cereb Cortex. 2016 Jan;26(1):288-303
18. Gu Y, Sainburg LE, Kuang S, Han F, Williams JW, Liu Y, Zhang N, Zhang X, Leopold DA, Liu X. Brain Activity Fluctuations Propagate as Waves Traversing the Cortical Hierarchy. Cereb Cortex. 2021 Jul 29;31(9):3986-4005.
19. Guedj C., Monfardini E., Reynaud A. J., Farnè A., Meunier M., and Hadj-Bouziane F., Boosting norepinephrine transmission triggers flexible reconfiguration of brain networks at rest, *Cerebral Cortex*. (2016) 27600848
20. Han F, Gu Y, Liu X. A neurophysiological event of arousal modulation may underlie fMRI-EEG correlations Front Neurosci 2019 13. 823
21. Huntenburg JM, Bazin PL, Margulies DS. Large-Scale Gradients in Human Cortical Organization. Trends Cogn Sci. 2018 Jan;22(1):21-31.
22. Hutchison RM, Womelsdorf T, Allen EA, Bandettini PA, Calhoun VD, Corbetta M, Della Penna S, Duyn JH, Glover GH, Gonzalez-Castillo J, Handwerker DA, Keilholz S, Kiviniemi V, Leopold DA, de Pasquale F, Sporns O, Walter M, Chang C. Dynamic functional connectivity: promise, issues, and interpretations. Neuroimage. 2013 Oct 15;80:360-78. doi: 10.1016/j.neuroimage.2013.05.079. Epub 2013 May 24.
23. Iraji A, Faghiri A, Lewis N, Fu Z, Rachakonda S, Calhoun VD. Soc Cogn Affect Neurosci. Tools of the trade: estimating time-varying connectivity patterns from fMRI data. 2021 Aug 5;16(8):849-874. doi: 10.1093/scan/nsaa114.
24. Keilholz SD, Magnuson ME, Pan WJ, Willis M, Thompson GJ. 2013. Dynamic properties of functional connectivity in the rodent. Brain Connect 3:31–40
25. Keilholz S, Caballero-Gaudes C, Bandettini P, Deco G, Calhoun V. Time-Resolved Resting-State Functional Magnetic Resonance Imaging Analysis: Current Status, Challenges, and New Directions. Brain Connect. 2017 Oct;7(8):465-481. doi: 10.1089/brain.2017.0543.
26. Koda K, Ago Y, Cong Y, Kita Y, Takuma K, Matsuda T (2010) Effects of acute and chronic administration of atomoxetine and methylphenidate on extracellular levels of noradrenaline, dopamine and serotonin in the prefrontal cortex and striatum of mice. J Neurochem 114:259 – 270.
27. Liu X, Duyn JH. Time-varying functional network information extracted from brief instances of spontaneous brain activity. Proc Natl Acad Sci U S A. 2013 Mar 12;110(11):4392-7.
28. Liu, T. T., Nalci, A., & Falahpour, M. (2017). The global signal in fMRI: Nuisance or Information?. Neuroimage, 150, 213-229.
29. Liu, X., de Zwart, J.A., Schölvinck, M.L. *et al.* Subcortical evidence for a contribution of arousal to fMRI studies of brain activity. *Nat Commun* **9**, 395 (2018).
30. Liu Y, Zhang N. Propagations of spontaneous brain activity in awake rats. Neuroimage. 2019 Nov 15;202:116176.
31. Lloyd, B., de Voogd, L. D., Mäki-Marttunen, V., & Nieuwenhuis, S. (2023). Pupil size reflects activation of subcortical ascending arousal system nuclei during rest. *ELife*, *12*, e84822.

32. Lurie, D. J., Kessler, D., Bassett, D. S., Betzel, R. F., Breakspear, M., Kheilholz, S., et al. (2020). Questions and controversies in the study of time-varying functional connectivity in resting fMRI. Netw. Neurosci. 4, 30–69. doi: 10.1162/netn_a_00116
33. McCormick, D. A., Nestvogel, D. B., & He, B. J. (2020). Neuromodulation of Brain State and Behavior. Annual review of neuroscience, 43, 391–415.
34. MacDowell CJ, Buschman TJ. Low-Dimensional Spatiotemporal Dynamics Underlie Cortex-wide Neural Activity. Curr Biol. 2020 Jul 20;30(14):2665-2680.e8.
35. MacDowell CJ, Tafazoli S, Buschman TJ. A Goldilocks theory of cognitive control: Balancing precision and efficiency with low-dimensional control states. Curr Opin Neurobiol. 2022 Oct;76:102606.
36. Matsui T, Murakami T, Ohki K. Transient neuronal coactivations embedded in globally propagating waves underlie resting-state functional connectivity. Proc Natl Acad Sci U S A. 2016 Jun 7;113(23):6556-61.
37. Meyer-Baese L, Watters H, Keilholz S. Spatiotemporal patterns of spontaneous brain activity: a mini-review. Neurophotonics. 2022 Jul;9(3):032209. doi: 10.1117/1.NPh.9.3.032209.
38. Mitra A, Kraft A, Wright P, Acland B, Snyder AZ, Rosenthal Z, Czerniewski L, Bauer A, Snyder L, Culver J, Lee JM, Raichle ME. Spontaneous Infra-slow Brain Activity Has Unique Spatiotemporal Dynamics and Laminar Structure. Neuron. 2018 Apr 18;98(2):297-305.e6.
39. Naci L, Cusack R, Anello M, Owen AM. A common neural code for similar conscious experiences in different individuals. Proc Natl Acad Sci U S A. 2014 Sep 30;111(39):14277-82.
40. O'Donnell, J., Zeppenfeld, D., McConnell, E., Pena, S., & Nedergaard, M. (2012). Norepinephrine: a neuromodulator that boosts the function of multiple cell types to optimize CNS performance. *Neurochemical research*, *37*, 2496-2512.
41. Pais-Roldán, P., Takahashi, K., Sobczak, F., Chen, Y., Zhao, X., Zeng, H., ... & Yu, X. (2020). Indexing brain state-dependent pupil dynamics with simultaneous fMRI and optical fiber calcium recording. *Proceedings of the National Academy of Sciences*, *117*(12), 6875-6882.
42. Power, J. D., Plitt, M., Laumann, T. O., & Martin, A. (2017). Sources and implications of whole-brain fMRI signals in humans. *Neuroimage*, *146*, 609-625.
43. Preti, T.A. Bolton, D. Van De Ville The dynamic functional connectome: state-of-the-art and perspectives. Neuroimage (2016)
44. Raut RV, Snyder AZ, Mitra A, Yellin D, Fujii N, Malach R, Raichle ME. Global waves synchronize the brain's functional systems with fluctuating arousal. Sci Adv. 2021 Jul 21;7(30):eabf2709.
45. Raut RV, Mitra A, Marek S, Ortega M, Snyder AZ, Tanenbaum A, Laumann TO, Dosenbach NUF, Raichle ME. Organization of Propagated Intrinsic Brain Activity in Individual Humans. Cereb Cortex. 2020
46. Raut RV, Rosenthal ZP, Wang X, Miao H, Zhang Z, Lee JM, Raichle ME, Bauer AQ, Brunton SL, Brunton BW, Kutz JN. Arousal as a universal embedding for spatiotemporal brain dynamics. BioRxiv
47. Rho, H. J., Kim, J. H., & Lee, S. H. (2018). Function of selective neuromodulatory projections in the mammalian cerebral cortex: comparison between cholinergic and noradrenergic systems. *Frontiers in neural circuits*, *12*, 47.

48. Rubinov M, Sporns O (2010) Complex network measures of brain connectivity: Uses and interpretations. NeuroImage 52:1059-69.
49. Shahsavarani S, Thibodeaux DN, Xu W, Kim SH, Lodgher F, Nwokeabia C, Cambareri M, Yagielski AJ, Zhao HT, Handwerker DA, Gonzalez-Castillo J, Bandettini PA, Hillman EMC. Cortex-wide neural dynamics predict behavioral states and provide a neural basis for resting-state dynamic functional connectivity. Cell Rep. 2023 Jun 27;42(6):112527. doi: 10.1016/j.celrep.2023.112527.
50. Shine JM, van den Brink RL, Hernaus D, Nieuwenhuis S, Poldrack RA. Catecholaminergic manipulation alters dynamic network topology across cognitive states. Netw Neurosci. 2018 Sep 1;2(3):381-396
51. Shine JM. Neuromodulatory Influences on Integration and Segregation in the Brain. Trends Cogn Sci. 2019 Jul;23(7):572-583.
52. Shine JM, Poldrack RA. Principles of dynamic network reconfiguration across diverse brain states. Neuroimage. 2018 Oct 15;180(Pt B):396-405.
53. Swanson CJ, Perry KW, Koch-Krueger S, Katner J, Svensson KA, Bymaster FP (2006) Effect of the attention deficit/hyperactivity disorder drug atomoxetine on extracellular concentrations of norepinephrine and dopamine in several brain regions of the rat. Neuropharmacology 50:755–760.
54. Tagliazucchi E, Balenzuela P, Fraiman D, Chialvo DR. Criticality in large-scale brain FMRI dynamics unveiled by a novel point process analysis. Front Physiol. 2012 Feb 8;3:15.
55. Timmermann, C., Roseman, L., Haridas, S., Rosas, F. E., Luan, L., Kettner, H., ... & Carhart-Harris, R. L. (2023). Human brain effects of DMT assessed via EEG-fMRI. Proceedings of the Nati*onal Academy of Sciences*, *120*(13), e2218949120.
56. G.J. Thompson, M.E. Magnuson, M.D. Merritt, et al. Short-time windows of correlation between large- scale functional brain networks predict vigilance intraindividually and interindividually. Hum Brain Mapp, 34 (2012), pp. 3280-3298
57. Totah, N. K., Neves, R. M., Panzeri, S., Logothetis, N. K., & Eschenko, O. (2018). The locus coeruleus is a complex and differentiated neuromodulatory system. *Neuron*, *99*(5), 1055-1068.
58. A.E. Urai, A. Braun, T.H. Donner. Pupil-linked arousal is driven by decision uncertainty and alters serial choice bias. Nat Commun, 8 (1) (2017), p. 1
59. Vafaii H, Mandino F, Desrosiers-Grégoire G, O'Connor D, Markicevic M, Shen X, Ge X, Herman P, Hyder F, Papademetris X, Chakravarty M, Crair MC, Constable RT, Lake EMR, Pessoa L. Multimodal measures of spontaneous brain activity reveal both common and cedivergent patterns of cortical functional organization. Nat Commun. 2024 Jan 3;15(1):229.
60. van den Brink R. L., Pfeffer T., Warren C. M., Murphy P. R., Tona K. D., van der Wee N. J., Giltay E., van Noorden M. S., Rombouts S. A., Donner T. H., and Nieuwenhuis S., Catecholaminergic neuromodulation shapes intrinsic MRI functional connectivity in the human brain, *The Journal of Neuroscience*. (2016) 36, no. 30, 7865–7876
61. van den Brink RL, Nieuwenhuis S, Donner TH. Amplification and Suppression of Distinct Brainwide Activity Patterns by Catecholamines. J Neurosci. 2018 Aug 22;38(34):7476-7491.
62. Van den Brink, Pfeffer, Donner. Brainstem Modulation of Large-Scale Intrinsic Cortical Activity Correlations. Front. Hum. Neurosci., 09 October 2019 Volume 13 – 2019

63. Wong CW, Olafsson V, Tal O, Liu TT. The amplitude of the resting-state fMRI global signal is related to EEG vigilance measures. Neuroimage. 2013
64. Wu GR, Colenbier N, Van Den Bossche S, Clauw K, Johri A, Tandon M, Marinazzo D. rsHRF: A toolbox for resting-state HRF estimation and deconvolution. Neuroimage. 2021 Dec 1;244:118591.
65. Xu, Y., Long, X., Feng, J. et al. Interacting spiral wave patterns underlie complex brain dynamics and are related to cognitive processing. Nat Hum Behav 7, 1196–1215 (2023).
66. Yin D, Kaiser M. Understanding neural flexibility from a multifaceted definition. Neuroimage. 2021 Jul 15;235:118027. doi: 10.1016/j.neuroimage.2021.118027. Epub 2021 Apr 6. PMID: 33836274.
67. Yousefi and Keilholz (2021) Propagating patterns of intrinsic activity along macroscale gradients coordinate functional connections across the whole brain. Neuroimage 213, 117827.